Simulation of Multiple-Antenna Terminal Performance in Massive MIMO Systems based on Indoor Measurements

Bengtsson, Erik L; Rusek, Fredrik; Edfors, Ove; Tufvesson, Fredrik; karlsson, Peter C.

Published in:
IEEE Transactions on Vehicular Technology

DOI:
10.1109/TVT.2019.2949738

2020

Simulation of Multiple-Antenna Terminal Performance in Massive MIMO Systems based on Indoor Measurements

Erik L. Bengtsson, Fredrik Rusek, Peter C Karlsson, Fredrik Tufvesson, Ove Edfors

***Abstract*—In massive MIMO systems the uplink pilot signals transmitted by a terminal define the channel seen by the base station. This gives the terminal some degree of freedom selecting an uplink pilot transmission strategy. In this paper, we investigate the benefit of different pilot transmission strategies when increasing the number of antennas in the terminal. Building on previous work on a simulation framework for Multiple-antenna terminals in 5G massive MIMO systems, this paper presents simulated performance results for various transmission schemes. The results are calibrated to reflect a real communication situation in a large auditorium. Emulating the measurement set-up, we show that the framework can be tuned to generate channel distributions that match measured data. Under generalized conditions, we perform simulations for different terminal transmission-strategies, both related to single stream and multiple streams. All evaluations are based on terminals with four antennas integrated into real Sony Xperia smartphone-chassis, tuned to 3.7 GHz. The measurements are conducted by using the Lund University Massive MIMO testbed with its 100 antennas. The results clearly show the advantage of increasing the antenna-count also at the terminal side in massive MIMO systems.**

***Index Terms*—Diversity, multiplexing, terminal antennas, massive MIMO, 5G, NR, channel model.**

I. Introduction

The immense growth in wireless communications and applications has led both to traffic congestion in the mobile frequency bands and an increased use of energy in the networks. Thus, the costs are escalating for operators as they try to meet the ever-increasing demands of the market. This, in turn, has spurred the research community to look for solutions to improve both the spectral and energy efficiencies of the communication systems. The most propitious technology, massive MIMO (MaMi) [1], promises improvements by several orders of magnitude for power efficiency and at least an order of magnitude for spectral efficiency, compared to single antenna systems [2]. Thanks to extensive research with promising results, most of the initial skepticism has settled [3] and MaMi is now emerging as one of the most promising components in the 5G new radio (NR).

This work is funded in part by Sony Mobile Communications in Lund, Sweden and Stiftelsen för Strategisk Forskning (SSF).

E.L. Bengtsson and F. Rusek are with Radio Access Lab, Sony Mobile communications in Lund, Sweden and with Lund University, department of Electrical and Information Technology, Sweden. email:erik.bengtsson@sony.com, fredrik.rusek@eit.lth.se

P.C Karlsson is with Radio Access Lab, Sony Mobile communications in Lund, Sweden. email:peterc.karlsson@sony.com

F. Tufvesson and O. Edfors are with Lund University, department of Electrical and Information Technology, Sweden. email: fredrik.tufvesson@eit.lth.se, ove.edfors@eit.lth.se

The main part of the MaMi research to date has focused on the base station (BS) with its, up to, hundreds of antennas. Noticeably, there are only a few publications that focus on the terminal perspective, and they show that terminals with multiple antennas can to a large extent influence the system performance [4]–[8]. In [6] we showed that besides antenna design, pilot transmission strategies will be crucial in MaMi systems.

The fundamental differences in terminal behavior are the motivation behind [8], a dedicated simulation framework with a reasonable complexity. The framework is designed for performance evaluation of multi-antenna terminals operated in a MaMi system. While it emulates the properties of a MaMi channel, as seen by a terminal, it avoids the complexity of a BS with its multitude of antennas. In the simulation framework, the environment is represented by only a few parameter settings. Random channels, distributed according to those expected form the environment of interest, are then obtained.

The channel properties within an environment not only depend on the position and orientation of a terminal but to a large portion on properties of the terminal antennas. Real integrated antennas with characteristics similar to those that can be expected in real products are therefore of essential importance in system evaluations. Multiple measurements with the same prototypes as used in [8] have shown that the distributions of the channel properties vary more than expected in seemingly similar environments. In fact, the locations of the clusters have a significant influence on the channel distribution for measurements limited to a few terminal orientations.

In this paper we conclude that, in order to achieve a good match between measured and simulated channel distributions the measurement scenario needs to be considered also in the simulation environment when estimating environmental parameters settings for the simulator.

It shall be noted that in this paper we investigate the advantage of having multiple antennas in a terminal. This is related to multiple-users (MU) sharing the same channel. The main differences are that in the MU case the signals at the different terminals can not be co-processed and that the antennas in different terminals can not be assumed to be physically static with respect to each-other. The consequences are that for the MU case the performance optimization relates to the BS side, and that the effective channel distributions become different. The influence MU has on the channel seen by a terminal will be addressed in our further work.

In this work, we use the simulation framework from [8] to

evaluate the advantage of increasing the antenna count at the terminal side, based on estimated environmental parameters. We examine received power and rate figures for different transceiver architectures and their associated pilot transmission strategies, for a quad-antenna terminal. As we consider handset terminals with the form factor of a spartphone, we do not consider it interesting with more than four antennas for the frequency band that we are investigating. This is also the number of antennas used in numerous products that can be found on the market, covering this frequency range.

The investigations are based on downlink received signals but the results are valid also for the uplink due to the reciprocity. Based on the large influence the terminal-antenna gain-patterns have on the link performance, we have used measured antenna gain-patterns from antennas integrated into a Sony Xperia ZL handset, tuned to 3.7 GHz, in all our evaluations[1]. We compare how the different antenna configurations perform in a MaMi system and investigate the advantage of having four antennas over one or two. The main contributions of this work are:

- The improved channel robustness obtained from scaling up the number of antennas at the BS side in a massive MIMO mainly relates to small scale fading. Our results clearly show an additional advantage of increasing the number of antennas also at the terminal side to address also large scale fading.
- Similar to conventional systems, asymmetric traffic, with higher downlink traffic than uplink traffic, makes it attractive to have a single transmit chain and multiple receive chains in the terminals. Our results suggest that this is feasible also for massive MIMO systems. For the single stream case, there is no need to have as many RF-chains as antennas, and switched solutions harvest most of the available capacity, also for this case.
- Contrary to conventional systems, the results confirm that opportunistic diversity approaches do not improve performance in a MaMi system.

In Section II we present the essential outcome from [8] and propose a method to derive typical channel parameter settings. We introduce the prototype based on which the simulations are performed and define different transmission schemes. In Section III we present simulation results where we compare SNR-gains for different diversity schemes and normalized-rate-gains for multiplexed schemes. Finally, in Section IV we conclude on the results.

II. Method

A. Framework for simulations

In this sub-section, we summarize the essential outcome of [8], a simulation framework used in this paper. The framework emulates the channel condition seen by the antennas of a terminal so that the received-signals, in a maximum-ratio-transmission (MRT) precoded MaMi system, can be computed. In the framework, it is assumed that the BS estimates channel state information based on uplink pilot-symbols transmitted from the terminal-antennas. This enables the BS to optimize the electrical field illuminating the terminal antennas in the downlink, as determined by channel properties and attributes of the pilot.

In [8] we made the following assumptions on which the framework is based:

- The multi-path-components (MPCs) are clustered.
- The BS do not have the resolution to control individual MPCs within a cluster.
- A cluster is defined by a center angle (CA), in azimuth and elevation, and an angular spread, also in azimuth and elevation, as seen from the terminal.
- The cluster gain function, and thus also the signal strength, of a cluster is constant within angles defined by the cluster.
- The center angles of clusters are uniformly distributed over the sphere, as seen by the terminal antennas.
- The cluster gain does not depend on polarization and does not favour any polarization direction.
- The BS can individually control power level, phase, and polarization of the signal to each cluster seen by the terminal.
- All clusters are in the far field as seen from the terminal antennas and they are therefore exposed to the same electrical field.

Based on above assumptions and that the framework only considers the conditions at the terminal side, the propagation-channel can be defined by only four parameters: the number of clusters, N; the angular spread, AS, of the illuminating field; and the standard deviation, C, of the cluster gain, λ. As we are not interested in the absolute channel strength we normalize the total power. Due to the normalization, the value of λ becomes indirectly defined by C, and is therefore not treated as a parameter in this work.

Fig. 1 shows the measured antenna-pattern of one antenna exposed to the electrical field built up of N clusters of multipath components. The electrical field only illuminates the terminal from the CA, indicated by red circles in the figure.

The relationship between a transmitted pilot signal and the associated received signal can be used by the terminal to gain access to the channel properties. With the antenna gain patterns defined by $\mathbf{\Psi}(\mathbf{\Omega})$, noise free conditions and the pilot set to unity[2] the received signal at terminal antenna k when a pilot signal has been transmitted from antenna l can be expressed as

[1]The reason for us to use the 3.7 GHz band is licensing, it is part of the spectrum identified for 5G in Europe (a.k.a. the 3.5 GHz band), and is used by the Lund University MaMi testbed, LuMaMi [9], [10]. LuMaMi is a real time testbed with 100 antennas which is also capable of capturing the complex channel coefficients based on up-link pilot signals transmitted from the terminals.PHY layer is similar to LTE, with 1200 sub-carriers over a 20 MHz BW, at 3.7 GHz

[2]Assuming MRT precoding at the BS side, the gain λ_n from a cluster n will influence the received signal twice. First, when the pilot is transmitted to the BS, and second, when the signal is propagated back to the terminal, through the same cluster, using MRT. Here we retain the square dependency to be able to observe the channel inner product directly. With the pilot signal set to unity, the relative magnitudes at each of the terminal antennas will, therefore, reflect those of the channel inner products, which carries essential behavior of a channel [11].

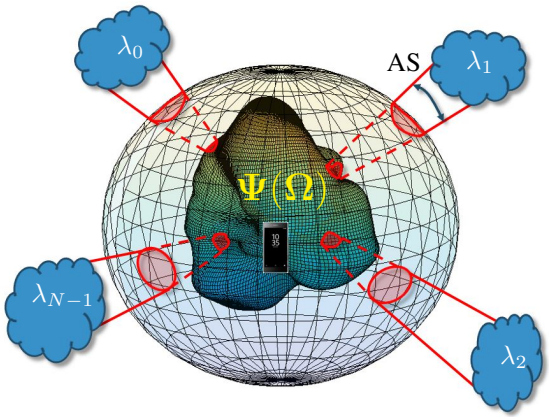

Fig. 1: N clusters with normalized cluster power λ_n and angular spread, AS, illuminating terminal antennas, with a measured gain pattern $\boldsymbol{\Psi}(\boldsymbol{\Omega})$.

$$y_{k|l} = \sum_{n=0}^{N-1} \lambda_n^2 \int_{\mathcal{A}_n} \int_{\mathcal{A}_n} \boldsymbol{\Psi}_k^{\mathrm{H}}(\boldsymbol{\Omega}_1) \boldsymbol{\Psi}_l(\boldsymbol{\Omega}_2) \mathrm{d}\boldsymbol{\Omega}_1 \mathrm{d}\boldsymbol{\Omega}_2, \qquad (1)$$

where $\boldsymbol{\Omega}$ is the directive angles and $\mathcal{A}_n$ the directive angles illuminated by cluster n. $\boldsymbol{\Psi}_l(\boldsymbol{\Omega})$ can be understood as being the illuminating E-field precoded by the BS, based on a pilot from antenna l. By complex weighing of the received signals from different antennas, exposed to the same electrical field, the received signal from the combined pattern from multiple antennas can be computed. The relative magnitudes at each of the terminal antennas, therefore, will reflect those of the channel inner products (the Gramian $\boldsymbol{G} = \boldsymbol{H}\boldsymbol{H}^{\mathrm{H}}$) which carries essential behavior of a channel [11], and from which the performance can be derived. The Gramian is given by

$$\boldsymbol{G} = \begin{bmatrix} y_{0|0} & y_{0|1} & \cdots & y_{0|K-1} \\ y_{1|0} & y_{1|1} & \cdots & y_{1|K-1} \\ \vdots & \vdots & \ddots & \vdots \\ y_{K-1|0} & y_{K-1|1} & \cdots & y_{K-1|K-1} \end{bmatrix}. \qquad (2)$$

Again, for a more thorough motivation we refer to our original work [8].

A large number of simulated channel realizations have been used to determine the distributions of the entries of $\boldsymbol{G}$. The simulations are defined by the following steps:

1) Measure the terminal antenna gain patterns, i.e. $\boldsymbol{\Psi}(\boldsymbol{\Omega})$, defined with a common center point.
2) Select the environmental parameters to reflect the environment of choice, i.e. N, C and AS.
3) Generate the vector $\boldsymbol{\lambda} = [\lambda_1 \ \lambda_2 \cdots \lambda_N]^{\mathrm{T}}$, where C is used as the standard deviation for the generation according to the approach in [12].
4) For each of the N clusters, define the integration area, $\mathcal{A}_n$, based on a random CA and the AS.
5) Compute the instantaneous Gramian (2).
6) Repeat steps 3) to 5) for the values defined in steps 1) and 2), to generate statistics of the Gramian.

Next we describe how to select pre-defined sets of parameters, for step two, that define a propagation environment.

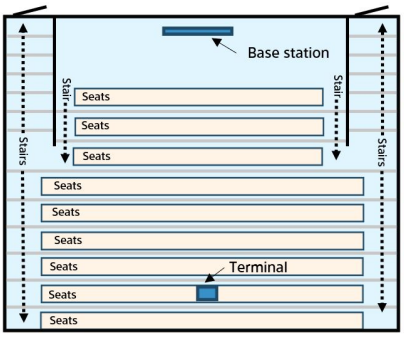

Fig. 2: Drawing of the auditorium where the measurements was performed. The terminal in the center of the room and the BS at the front.

B. Environmental settings

In this sub-section, we compare simulated channels to measured channels and motivate our choice of environmental parameters. Both simulated and measured results are generated using the same dual-antenna terminal.

The measurements were performed in an auditorium, as shown in Fig. 2. The location was chosen since earlier measurement campaigns have been performed in the same environment [13], providing prior knowledge of the channel properties. The environment is considered indoor based on the scattering properties, e.g., from walls, roof, and furnitures. While the terminal was measured in different locations in the room the MaMi BS was fixed to the front center. We used an absorbent to block the line-of-sight component between the BS and the terminal, mainly due to limitations in the dynamic range of the measurements. By only rotating the terminal, keeping it at the same location while monitoring channel properties, all channel variations can be assumed to be determined by the terminal antenna properties, as the propagation channel in that case can be assumed to be static. For the measurements, the terminal was rotated in steps of about 10°and the full channel, $\boldsymbol{H}$, captured at the BS side.

For the comparison between measured and simulated channel distributions we limit the study to the two-antenna case, while the simulation study to follow handles up to four antennas.

For the comparison, we present a channel measured in the back of the room and represent it by the power imbalance β and correlation α. From a fundamental perspective, the imbalance β is a relative measure of a channel realization that tells how strong channel the different antenna sees, while α indicates how much cross-talk there are. α and β represent a normalized channel realization and their distributions is, therefore, a measure on the channel behaviour for an environment.

For each simulated channel realization, we compute the normalized Gramian, $\boldsymbol{G}_{\mathrm{norm}} = \frac{2}{\mathrm{tr}\{\boldsymbol{G}\}}\boldsymbol{G}$ (where $\mathrm{tr}\{\cdot\}$ is the trace operator). From $\boldsymbol{G}_{\mathrm{norm}}$ we get access to the relevant channel properties, which do not depend on the precoding, and for the special case of two antennas, the power imbalance β and correlation α [14] can be identified from

$$\boldsymbol{G}_{\mathrm{norm}} = \begin{bmatrix} 1+\beta & \alpha \\ \alpha* & 1-\beta \end{bmatrix}. \qquad (3)$$

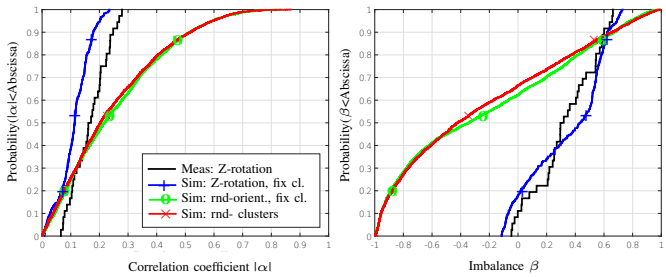

Fig. 3: CDFs of correlation coefficient $|\alpha|$ and imbalance β for measurements and simulations with different settings.

In measurements, the pilots transmitted by the terminal antennas, give direct access to the experienced channel, $\boldsymbol{H}$, from which, we can straightforwardly compute the Gramian and further identify α and β after normalization.

It can be understood from Fig. 1, that the antenna gain for integrated terminal antennas will change dramatically as a function of the illumination angle. As much as this is one of the most important motivations for doing investigations with realistic integrated antennas, it also poses challenges. As mentioned, large variations in the received signal power as the terminal is illuminated from different angles can be expected. This will then also show up in the channel distributions, i.e. distributions of α and β, making it hard to isolate environment specific properties. Measurements performed at different locations and environments confirm this. The distributions of α and β depend as much on the environment as on the orientation of the terminal. Even if possible, extracting typical parameters for an environment is a very tedious task that involves tremendous measurement efforts for each environment.

To verify the validity of the simulation framework and keep the measurement effort reasonable, simulated α and β distributions have been matched to those measured at a single location where a terminal was rotated only around the vertical axis. We have matched the simulated results to those measured according to the maximum likelihood (ML) principle, under the assumption that the correlation coefficient, $\alpha' = |\alpha|/(\sqrt{1-\beta^2})$ and β are independent.

By restricting the simulator to rotation around the same axis as for the measurements and, with a careful selection of azimuth and elevation angles for a set of two clusters, the distributions of α and β could be significantly better matched to the measured distributions. Fig. 3 shows the distributions of α and β coloured black and blue. The distributions demonstrate that the simulation framework is capable of generating realistic distributions that reflect a specific scenario. However, they also indicate that the distributions are very sensitive to how the terminal is oriented with respect to the clusters. Indeed, by keeping the clusters' relative angles fixed in the simulator, while randomly changing the orientation of the terminal, not limited to rotation along any axis, the distributions change dramatically. This is shown as the red curves in Fig. 3. While not unexpected, an important observation is that by setting the cluster angles randomly the distribution matches the one with the fixed clusters and random orientations. This is shown as the green curves in Fig. 3. All in all, those results suggest that random selection of the illumination angles yields representative channels in most cases and therefore makes the simulated distributions of antenna gain and correlation more generic. Hence, illumination angles will be different for different positions and the results show that random illumination angles give the same result as fixed clusters and random orientation of the terminal.

Being confident that the simulation framework generates sufficiently realistic channel realizations we continue our analysis. Initially, we set the number of clusters to $N = 2$, the AS to 12° and the cluster gain standard deviation C=0 dB, motivated by that this is what multiple measurements in different locations of the room suggested. It may be argued that expected number of clusters in this environment is larger than the two we observed [13]. A plausible explanation to the low number is that the channel behaviour is mainly determined by a few dominant clusters and the influence from weaker clusters in this setting is negligible. The effect of introducing variation to the normalized cluster power is, therefore, mainly the same as reducing the number of clusters for the single user case, and will not be further treated in this paper. In fact, we are not attempting to estimate the number of clusters but rather to find the settings that generate realistic channel distributions that match those measured. This is possible as we are limiting the investigation to the dynamic properties of the channel and do not consider the absolute level, which, is expected to vary significantly. The effect of the number of clusters on the received signals will be examined below. However, the physical size (i.e., AS) of the clusters has a negligible influence, within the range 6° to 18°, and will therefore be set to a fixed value. The influence of the AS relates to the angular variation in the antenna gain patterns, which in our case can be considered small.

C. Terminal antenna configurations and performance metrics

For the simulation study, we investigate an Xperia ZL smartphone with four integrated antennas, as shown in Fig. 4. This set-up enables us to evaluate six combinations of antenna pairs as well as the case of all four antennas used simultaneously. Two of the antennas in the Xperia ZL prototype are placed in the upper end, right (R) and left (L), one in the bottom (B) and one at the side (S). The prototype is equipped with switches to pair-wise select any two of the antenna pair combinations. All antenna gain-patterns have been measured in a Satimo StarGate 64 anechoic chamber for both free-space (FS) and loaded conditions. The loaded case, is a combination of; left-hand; right-hand; beside-head-with-left-hand; and beside-head-with-right-hand. The results are generated by combining the distributions generated by the different load-cases. The load-cases are selected from the perspective that they offer repeatability rather than being typical 5G use cases.

To compare the different antenna configurations on an equal basis, without the insertion loss from the switch circuitry, the received power for each antenna configuration has been normalized with the average of the median power of all four

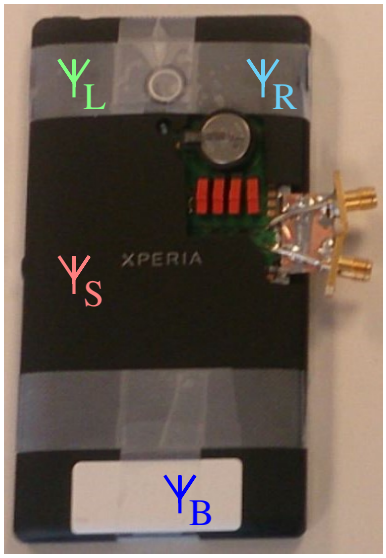

Fig. 4: Xperia ZL with antenna positions indicated.

antennas under FS conditions, i.e.

$$P_{\text{ref}} = \frac{1}{4} \sum_{k \in \{L,R,S,B\}} \tilde{\text{m}} \left(y^2_{\text{FS-k|FS-k}} \right), \tag{4}$$

where $\tilde{\text{m}}(\cdot)$ denotes the median operator and with y from (1). To simplify the notation, we relate k to the antennas rather than using an integer. The normalized power for e.g. the loaded top-right antenna is given by

$$P_{\text{Load-R}} = \frac{y^2_{\text{load-R|load-R}}}{P_{\text{ref}}}. \tag{5}$$

The simulator directly yields the Gramian (2). From the Gramian, the performance of different transmission schemes can be computed and below we put forth our selection of schemes. For the comparison of different diversity schemes, we use SNR-gain [6]. The SNR-gain shows how much the signal-to-noise-ratio (SNR) is improved by a certain scheme and is defined as the ratio between the received power achieved by a diversity scheme to that of a single antenna, for the same channel realization. Each channel realization will therefore generate as many SNR-gains as there are antennas. In the result section below we combine all those SNR-gains from a large number of realizations into a single distribution. In general, the transmission schemes below define the performance for both uplink and downlink. Passive receive diversity as described below, however, only operates in the downlink.

D. Single stream schemes

1) Passive receive diversity (PD): The PD scheme is limited to single stream transmissions. The terminal has a single transmit antenna and multiple receive antennas. As the terminal only transmits pilots from one antenna, the BS does not get access to the full channel, and can only optimize transmissions to the same antenna. We define one transmit/receive antenna, i, and three receive-only antennas. The quality of the received signal after maximum ratio combination, without any noise enhancement is given by

$$y_{\text{PD}(i)} = \|\boldsymbol{t}_i \boldsymbol{G}\|, \tag{6}$$

where the vector $\boldsymbol{t}_i$, a vector of zeros with a one at the column i, reflects which antenna transmitted the pilot signal and thus defines the channel the BS sees.

2) Switched diversity (SWD): In SWD we use a switch to select one antenna among the available ones for each channel realization. The SWD scheme is limited to transmit and receive a single stream. We use only one of the antennas at the time, but we have all four antennas to switch among. The received signal is given by

$$y_{\text{SWD}} = \max(y_{0|0}, y_{1|1}, y_{2|2}, y_{3|3}), \tag{7}$$

where the antenna with the strongest signal is selected.

Dominant Eigenmode (DEM) schemes, like the PD and SWD schemes, are also limited to a single stream. The DEM schemes involve all available antennas for both uplink and downlink and require as many transceiver chains as there are available antennas. We study two variants, limited by different transceiver architectures.

3) Dual antenna, dominant Eigenmode (DEM2): DEM2 transmission involves two antennas (i and j). The received signal is given by

$$y_{\text{DEM2}(ij)} = \max(\text{eig}\{\boldsymbol{G}_{i,j}\}), \tag{8}$$

where $\text{eig}\{\cdot\}$ is the operator that computes the eigenvalues of a matrix and $\boldsymbol{G}_{i,j}$ is a 2×2 sub-matrix of (2), given by

$$\boldsymbol{G}_{i,j} = \begin{bmatrix} y_{i|i} & y_{i|j} \\ y_{j|i} & y_{j|j} \end{bmatrix}, \tag{9}$$

where $y_{i|j}$ are the elements of the Gramian, $\boldsymbol{G}$ at row i and column j.

4) Quad-antenna dominant Eigenmode (DEM4): This scheme involves all four antennas simultaneously. The received signal using the single most dominant eigenmode is given by

$$y_{\text{DEM}} = \max(\text{eig}\{\boldsymbol{G}\}). \tag{10}$$

The DEM4 scheme is the optimal scheme from a power transfer perspective and will be used as reference in comparisons later on. Note, contrary to the two antenna case, we need the complex received signals in the Gramian (2) when deriving the eigenvalues.

E. Multiplexed transmission (MUX)

Multiplexed transmission involves having multiple, simultaneous, and independent streams. In order to compare MUX schemes with diversity schemes on an equal basis, the received signal for each independent stream needs to be related to a rate. The reason for this is that we can sum the rates and compare to the rate of the diversity schemes. This is not possible with SNR-gains.

The capacity of a stream m is given by $\mathcal{C}_m = \log_2(1 + \text{SNR}_m)$, where SNR_m is the ratio between a normalized received power, with the same normalization as in (5), P_m and an absolute noise power, N_0. We define our reference SNR to be the ratio between the average of all antenna's median power in FS, defined in (4), to the absolute noise power.

The sum rate offered by M streams with transmit-power constrained to unity is given by

$$\mathcal{C}_M = \max_{\sum_{m=1}^{M} a_m = 1} \sum_{m=1}^{M} \log_2 \left(1 + \frac{a_m P_m}{N_0}\right), \qquad (11)$$

where $a_m \geq 0$ and P_m are the power scaling factor and the normalized power level for stream m. The water pouring algorithm [15] is used to compute (11). We will now define three MUX schemes.

1) Dual antenna multiplexed transmission (MUX2): This scheme is similar to the DEM2 scheme but uses two simultaneous independent streams by addressing both eigenmodes of the channel. The received signals for the streams, based on antennas i and j, are given by

$$y_{\text{MUX2}(1,ij)} = \max(\text{eig}\{\boldsymbol{G}_{i,j}\}), \qquad (12)$$

and

$$y_{\text{MUX2}(2,ij)} = \min(\text{eig}\{\boldsymbol{G}_{i,j}\}). \qquad (13)$$

The rate, $\mathcal{C}_{\text{MUX2(ij)}}$, is then given by (11), where the signals are converted to powers.

2) Switched, dual antenna multiplexed transmission (MUX2SW): Like the MUX2 scheme, this scheme involves two antennas simultaneously. For each realization the achieved rates for all six combinations of antenna pairs are computed and the best pair is selected. We define

$$\mathcal{C}_{\text{MUX2SW}} = \max(\mathcal{C}_{\text{MUX2}(01)}, \mathcal{C}_{\text{MUX2}(02)}, \cdots, \mathcal{C}_{\text{MUX2}(23)}). \qquad (14)$$

3) Dual-stream, eigenmode based multiplexed transmission (MUX2DEM): This scheme is similar to the MUX2 scheme but uses all four antennas. The received signal from each of the received streams is given by

$$y_{\text{MUX}(m)} = \boldsymbol{F}_m \text{eig}\{\boldsymbol{G}\}, \qquad (15)$$

where $\boldsymbol{F}_m$ addresses stream $m \in \{1, 2\}$, being a row vector of zeros with a one at column m and $\text{eig}\{\boldsymbol{G}\}$ is a vector of eigenvalues derived from the complex received signals. This scheme is optimal from a dual stream conditioned rate perspective. To compute the rate we use (11).

4) Quad-stream multiplexed transmission (MUX4): The MUX4 scheme is a four stream scheme, similar to the MUX2DEM scheme but uses all four eigenmodes. The received signal from each of the received streams is given by (15) where $m \in \{1, 2, 3, 4\}$. This scheme is optimal from a rate perspective for each channel realization and reach capacity. To compute the rate we use (11).

The different transmission schemes presented above are summarized in Table I for easy reference. The number of receive (Rx) and transmit (Tx) chains in the third column is of interest as they relate to power consumption and hardware complexity.

TABLE I: List of transmission schemes.

Acronym	Scheme	Number of Rx-/Tx-chains	Streams (Rank)
PD	4 ant. passive Rx div.	4 / 1	1
SWD	4 ant. switced div.	1 / 1	1
DEM2	2 ant. dominant eigenmode div.	2 / 2	1
DEM4	4 ant. dominant eigenmode div.	4 / 4	1
MUX2	2 ant. multiplexing	2 / 2	2
MUX2SW	4 ant. SWD / 2 antenna MUX	2 / 2	2
MUX2DEM	4 ant. dual stream	4 / 4	2
MUX4	4 ant. quad stream	4 / 4	4

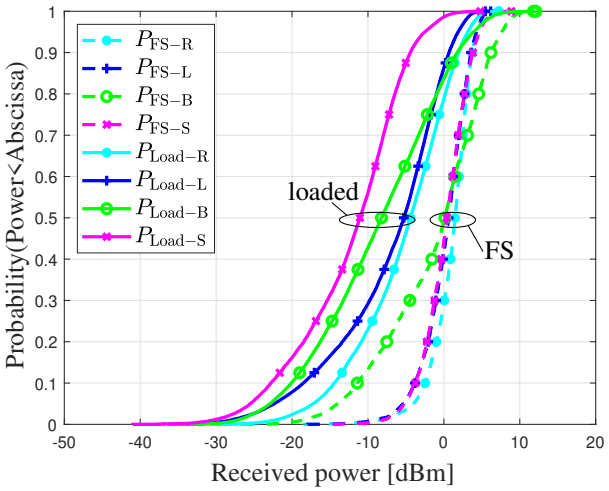

Fig. 5: Simulated CDFs of the normalized received power for each of the four antennas, FS and loaded conditions.

III. Simulation Results

Based on the measured loaded antenna patterns and the presented simulation-framework, SNR-gains and normalized-rate-gains have been simulated. The performance of the different diversity schemes can be visualized by plotting cumulative distribution functions (CDFs) of the received power.

Fig. 5 shows the CDFs of the received power at the four antennas, both under FS and loaded condition after the power normalization. The CDFs are generated from 5000 channel realizations for each load case, with the environmental parameters set to 2 clusters, an AS of 12°and a cluster gain standard deviation of 0 dB. The median and standard deviations are listed in Table II. Antenna B shows larger standard deviation than the other antennas in FS condition. This is a result of the antenna design resulting in a higher directive gain. Under the loaded condition, the standard deviation of the received powers for all antennas increase, again due to an increased directive gain. The median of the received power becomes lower in the loaded cases. The 7 dB drop is mainly caused by absorption as the matching is good for all our cases.

Fig. 6 shows CDFs for a selection of diversity schemes as well as CDFs of the received power at each of the antennas when no diversity is applied. The latter curves almost fully overlap the PD curves. The figure shows the performance for loaded conditions only, as we consider FS being less realistic. For the PD scheme, the performance improvement is negligible despite all four antennas being used. More interesting is that the SWD schemes perform about the same as the DEM4 scheme, the latter being optimal from a power transfer perspective. This suggests that in a majority of realizations the DEM4 scheme directs almost all power to a single antenna.

TABLE II: Simulated median and standard deviation of received power for the four antennas in FS and loaded.

Antenna	Median	Standard deviation
FS-L	1.5 dBm	2.8 dB
FS-R	0.6 dBm	3.0 dB
FS-B	0.1 dBm	6.7 dB
FS-S	0.4 dBm	3.0 dB
Load-L	-4.4 dBm	6.3 dB
Load-R	-5.2 dBm	7.4 dB
Load-B	-8.2 dBm	8.2 dB
Load-S	-11.1 dBm	7.1 dB

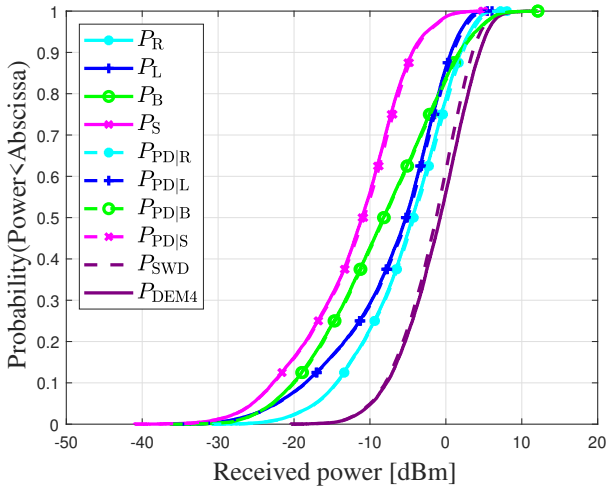

Fig. 6: Simulated CDFs of the received normalized power for the different diversity schemes under loaded conditions. The four R, L, B, and S curve pairs $P_{\cdot}$ and $P_{PD|\cdot}$ are essentially placed on top of each other.

This can be explained by low correlation between the antennas, as will be confirmed with the MUX schemes below.

A. SNR-Gain

The SNR-gains are defined as a ratio between the received power achieved by a scheme to that with a single antenna, P_{SA}. With four antennas available, each realization therefore generates four results where each of the antennas is used as reference. Fig. 7 shows CDFs where the four distributions are combined. Consequently, as at least one antenna will always be the best and when it used as reference the gain becomes lower. This explains why the SNR-gain CDF for the SWD scheme shows 0 dB gain in 25% of the realizations. The low correlation between the antennas in combination with the MaMi precoding has a large impact on the performance. This is the reason to the negligible SNR-gain from the PD scheme (shown as a combined CDF for all cases), which is less than 0.25 dB in the 90 percentile, and also the reason to why the SWD scheme performs close to the DEM4 scheme.

For the DEM2 schemes, we show the CDFs for all 6 antenna combinations as well as the combined CDF. When we limit the transmissions to any of the antenna pairs, the loss is significant. This, clearly show that there is an advantage to have access to all four antennas.

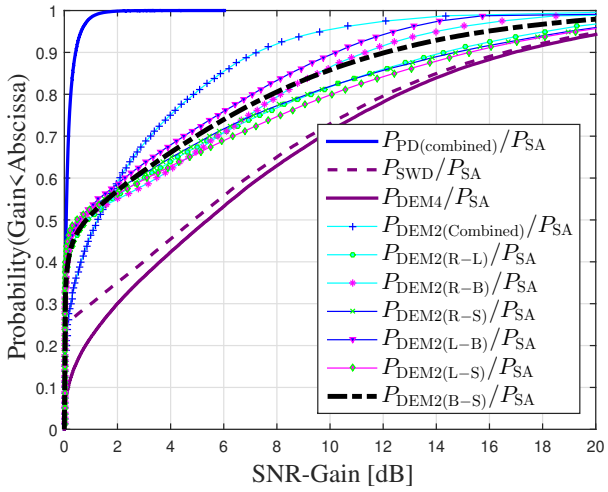

Fig. 7: CDFs showing the SNR-gains for the different diversity schemes.

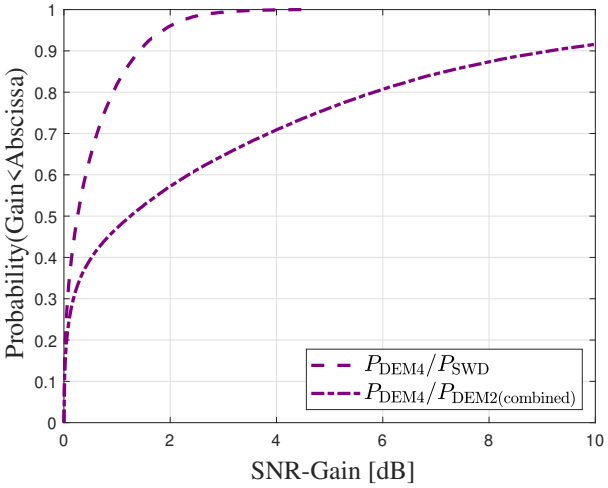

Fig. 8: CDFs showing the SNR-gain ratio.

To get a more quantitative comparison between the different schemes, SNR-gain ratios have been derived. Fig. 8 shows the SNR-gain ratios between a selection of schemes to that of the DEM4 scheme (optimal). We can conclude that the SWD scheme is less than 1.5 dB from being optimal at the 90 percentile. For the DEM2 scheme, however, in 20% of the cases, it is more than 6 dB below the optimal.

B. Sum rate comparison

To include the MUX schemes in this comparison, we will now plot rate CDFs. Fig. 9 shows rate CDFs for a selection of schemes, at a reference SNR of 10 dB with unity power transmitted.

In general, increasing the number of streams yields a higher rate. Interestingly, the MUX2 scheme (all 6 combinations presented in a combined CDF), where we limit the transmissions to any two of the antennas, often show lower rates than the

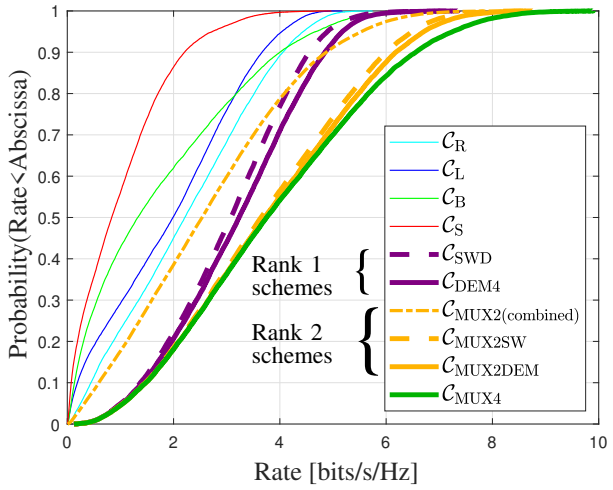

Fig. 9: CDFs showing the rates at an SNR of 10 dB.

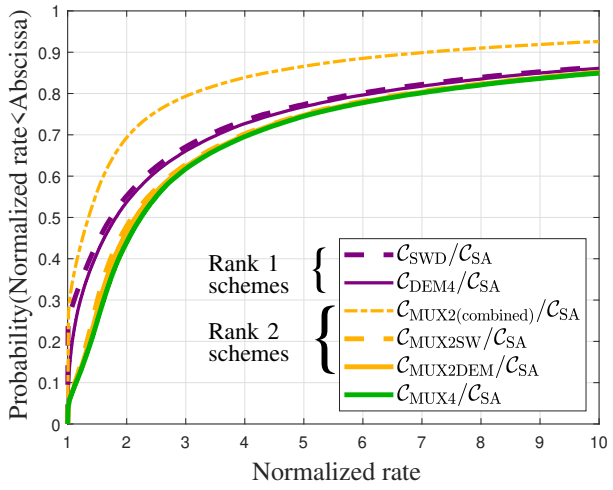

Fig. 10: CDFs showing the rate, normalized to that of single antenna operation, at an SNR of 10 dB.

SWD scheme. This, highlights the importance of having access to more antennas and again, is a result of the low correlation between the antennas.

Similar to the SNR-gain, we express the performance as a normalized rate, where we use the capacity given by each antenna as the reference and then combine the CDFs. Fig. 10 shows CDFs of the normalized rate for a selection of schemes. The results show the same trend as for the diversity schemes, namely, increasing the antenna count is more important than having a transceiver for each antenna. The difference between the DEM4 and the MUX2DEM schemes comes from the fact that the MUX2DEM scheme addresses both eigenmodes while the DEM4 scheme selects the strongest one. The results, however, depend heavily on the SNR and, intrinsically when the SNR increases, the ratio between the rates for different schemes converges. The ratio of the rates from any of the dual-stream schemes (i.e. MUX2SW and MUX2DEM) converges to two and from the quad-stream scheme (i.e. MUX4) to four as they are divided by the rate of any of the single stream schemes.

To find the operational range where the different MUX schemes are most effective, for each channel realization, the ratio between each of the MUX schemes and the DEM4 scheme was computed and the median of the resulting ratio-distribution derived. Fig. 11 shows the median of the normalized rate-ratios for $\mathcal{C}_{\mathrm{MUX4}}/\mathcal{C}_{\mathrm{DEM4}}$, $\mathcal{C}_{\mathrm{MUX2SW}}/\mathcal{C}_{\mathrm{DEM4}}$, $\mathcal{C}_{\mathrm{MUX2DEM}}/\mathcal{C}_{\mathrm{DEM4}}$ and $\mathcal{C}_{\mathrm{SWD}}/\mathcal{C}_{\mathrm{DEM4}}$ as functions of the SNR. The dashed line at an SNR of 10 dB indicates the level at which the previous plots where generated.

It should be noted that the channel properties used in the simulations are derived from measurements based on a dual-antenna terminal and, therefore, may not be entirely representative for simulation of four multiplexed streams. Depending on the precoder at the BS side, also weaker clusters may be heavily illuminated and the channel at the terminal side may therefore be perceived as richer. The Fig. 11 includes the impact of channel richness, in terms of number of clusters ranging from 2 to 6, where the normalized-rate-ratio increases with the number of clusters. For the sake of simplicity, we have used equally strong clusters in our simulations, which may not be entirely realistic but serves as an (upper) reference level. As the MUX4 scheme is optimal and reaches capacity, it may seem that this is the obvious choice in all cases. In a real scenario, however, a detector has an SNR limit, below which it can not operate. For the MUX schemes all streams need to have an SNR above this minimum level (which can be implemented in the water pouring algorithm). The plots in Fig. 11 are generated with the detection limit set to $-\infty$ dB, the schemes therefore show normalized rate-ratios larger than 1 also at unrealistically low SNRs.

For SNRs around 10 dB, the dual-stream schemes and the MUX4 schemes show only a small difference at lower number of clusters. In general, the MUX4 scheme shows a larger dependency on the number of clusters and has a significant advantage at SNRs beyond 10 dB. The SWD and MUX2SW schemes both are on par with their optimal counterpart the DEM4 and MUX2DEM schemes respectively. This shows the importance of having access to all antennas and that it is enough to reach close the rank conditioned capacity. A general conclusion is that, to reach a rate improvement of a factor of four, for the MUX4 scheme, the minimum SNR is about 20 dB higher than that of rate one. For the two stream schemes it is about 15 dB higher.

It can be generally stated that the switched schemes perform close to the rank conditioned capacity and this is the case also when the channel richness increases. It is naturally possible to find environments with other properties. However, we think that the environment that we selected can be considered representative for indoor propagation channels. By normalizing the propagation channels, and study dynamic properties rather than absolute levels our results show that it is mainly the number of clusters that determine the performance. As we see similar behaviour for various number of clusters we therefore assume that our conclusions are general. Furthermore, the results relies also on the antenna implementations. We believe that antennas integrated into the form-factor of a smartphone will be similar. Finally, the results are also based on how well

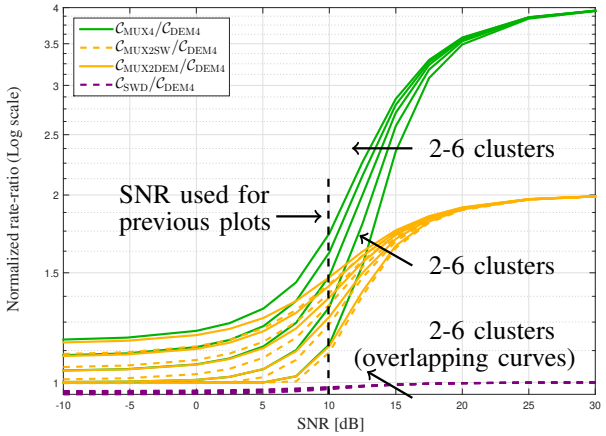

Fig. 11: Normalized rate vs. the SNR and the number of clusters. The clusters are in the range 2 to 6 and a larger number yield a higher ratio.

a channel can be accurately modelled with clusters, which was evaluated in [13].

IV. Discussion and Conclusion

The correlation between integrated handset-antennas tuned to the frequency range 2-6 GHz, is typically low. This, has a large influence on the rate and the SNR-gain different pilot transmission strategies return in a massive MIMO system. Our results show that switched architectures reach close to the rank-conditioned capacity of a channel and that having access to more antennas is essential.

Based on the asymmetric traffic in today's networks, a switch will not only be needed to enable uplink pilot transmission from all antennas, which is mandatory for massive MIMO systems but, the solution will be close to optimal from an uplink power transfer perspective.

The simulations also clearly show that the passive diversity- or MIMO-receivers, mandatory for LTE, will not provide optimal performance in a massive MIMO system, e.g. emerging 5G NR radio access, due to lack of pilot transmission capability from all antennas.

The simulation results further show that, at lower SNRs the benefit of multiplexed operation is limited and similar rates can be achieved with less complex switched diversity. Even if a terminal is equipped with receive and /or transmit chains to support both the dominant eigenmode and the multiplexed schemes with two or more streams there is a lot of power that can be saved by turning the transceiver chains off and use switched diversity instead, both from a computational complexity and power consumption perspective.

We show that there is a large difference between channel distributions generated by random terminal-orientations and those limited by few spherical cuts for a terminal with integrated antennas. It is important to pay attention to this difference when estimating channel properties from measured data.

V. Acknowledgment

The authors would like to thank Sony Mobile Communications in Lund, Sweden and Stiftelsen för Strategisk Forskning (SSF) for funding the project. The authors would also like to thank unnamed reviewers for their valuable contributions.

References

[1] T. L. Marzetta, "Noncooperative Cellular Wireless with Unlimited Numbers of Base Station Antennas OFDM," *IEEE Trans. Wireless Commun.*, vol. 9, no. 11, pp. 3590–3600, Nov. 2010, doi: http://dx.doi.org/10.1109/TWC.2010.092810.091092.

[2] H. Q. Ngo, E. G. Larsson, and T. L. Marzetta, "Energy and Spectral Efficiency of Very Large Multiuser MIMO Systems," *IEEE Transactions on Communications*, vol. 61, no. 4, pp. 1436–1449, Apr. 2013, doi: http://dx.doi.org/10.1109/TCOMM.2013.020413.110848.

[3] E. Björnson, E. G. Larsson, and T. L. Marzetta, "Massive MIMO: 10 Myths and One Critical Question," *IEEE Communications Magazine*, pp. 114–123, Feb. 2016, doi: http://10.1109/MCOM.2016.7402270.

[4] E. Björnson, J. Hoydis, M. Kountouris, and M. Debbah, "Massive MIMO Systems with Non-Ideal Hardware: Energy Efficiency, Estimation, and Capacity Limits," *IEEE Transactions on Information Theory*, vol. 60, no. 11, pp. 7112–7139, Nov. 2014, doi: http://dx.doi.org/10.1109/TIT.2014.2354403.

[5] E. L. Bengtsson, F. Tufvesson, and O. Edfors, "UE Antenna Properties and Their Influence on Massive MIMO Performance," in *Proceedings of the 9th European Conference on Antennas and Propagation, (EUCAP)*, Lisbon, Portugal, Apr. 2015.

[6] E. L. Bengtsson, P. C. Karlsson, F. Tufvesson, J. Vieira, S. Malkowsky, L. Liu, F. Rusek, and O. Edfors, "Transmission Schemes for Multiple Antenna Terminals in Real Massive MIMO System," in *Proceedings of GlobeCom 2016 Conference, IEEE Communications Society*, Washington DC, USA, Dec. 2016.

[7] À. O. Martínez, P. Popovski, J. Ø. Nielsen, and E. D. Carvalho, "Experimental Study of the Benefits of a Second Antenna at the User Side in a Massive MIMO System," *IEEE Access*, vol. PP, no. 99, pp. 1–1, 2017, doi: http://dx.doi.org/10.1109/ACCESS.2017.2785860.

[8] E. L. Bengtsson, F. Rusek, S. Malkowsky, F. Tufvesson, P. C. Karlsson, and O. Edfors, "A Simulation Framework for Multiple-Antenna Terminals in 5G Massive MIMO Systems," *IEEE Access*, vol. 5, pp. 26 819–26 831, 2017, doi: http://dx.doi.org/10.1109/ACCESS.2017.2775210.

[9] J. Vieira, S. Malkowsky, K. Nieman, Z. Miers, N. Kundargi, L. Liu, I. Wong, V. Öwall, O. Edfors, and F. Tufvesson, "A Flexible 100-Antenna Testbed for Massive MIMO," in *Globecom Workshops (GC Wkshps)*, 2014, pp. 287–293.

[10] S. Malkowsky, J. Vieira, L. Liu, K. Nieman, N. Kundargi, I. Wong, F. Tufvesson, V. Öwall, and O. Edfors, "The Worlds First Real-Time Testbed for Massive MIMO: Design, Implementation, and Validation," *IEEE Access*, vol. 5, pp. 9073 – 9088, May. 2017, doi: http://dx.doi.org/10.1109/ACCESS.2017.2705561.

[11] A. Paulraj, R. Nabar, and D. Gore, *Introduction to Space-Time Wireless Communications*, 1st ed. Cambridge University Press, 2003.

[12] *Universal Mobile Telecommunications System UMTS Spatial channel model for Multiple Input Multiple Output MIMO simulations*, 12th ed., ETSI, 3GPP TR 25.996, 2014.

[13] X. Gao, J. Flordelis, G. Dahman, F. Tufvesson, and O. Edfors, "Massive MIMO Channel Modeling - Extension of the COST 2100 Model," 2015.

[14] X. Gao, F. Tufvesson, O. Edfors, and F. Rusek, "Measured Propagation Characteristics for Very-Large MIMO at 2.6 GHz," in *Proc. of Asilomar Conference on Signals, Systems and Computers (ASILOMAR)*, Nov. 2012, pp. 295–299, doi: http://dx.doi.org/10.1109/ACSSC.2012.6489010.

[15] T. Cover and J. Thomas, *Elements of Information Theory*, 2nd ed. Wiley-Interscience, 2006.